Published in final edited form as:
Cell. 2008 November 28; 135(5): 933–947. doi:10.1016/j.cell.2008.10.011.

Real-time Redox Measurements during Endoplasmic Reticulum Stress Reveal Interlinked Protein Folding Functions

Philip I. Merksamer[1,2,3], **Ala Trusina**[1,2,3], and **Feroz R. Papa**[1,2,3,*]

[1]Department of Medicine, University of California, San Francisco, San Francisco, CA 94143-2520. U.S.A., Tel: 415-476-2117, FAX: 415-514-9656

[2]Diabetes Center, University of California, San Francisco, San Francisco, CA 94143-2520. U.S.A., Tel: 415-476-2117, FAX: 415-514-9656

[3]California Institute for Quantitative Biosciences, University of California, San Francisco, San Francisco, CA 94143-2520. U.S.A., Tel: 415-476-2117, FAX: 415-514-9656

SUMMARY

Disruption of protein folding in the endoplasmic reticulum (ER) causes unfolded proteins to accumulate, triggering the unfolded protein response (UPR). UPR outputs in turn decrease ER unfolded proteins to close a negative feedback loop. However, because it is infeasible to directly measure the concentration of unfolded proteins *in vivo*, cells are generically described as experiencing "ER stress" whenever the UPR is active. Because ER redox potential is optimized for oxidative protein folding, we reasoned that measureable redox changes should accompany unfolded protein accumulation. To test this concept, we employed fluorescent protein reporters to dynamically measure ER redox status and UPR activity in single cells. Using these tools, we show that diverse stressors, both experimental and physiological, compromise ER protein oxidation when UPR-imposed homeostatic control is lost. Using genetic analysis we uncovered redox heterogeneities in isogenic cell populations, and revealed functional interlinks between ER protein folding, modification, and quality control systems.

INTRODUCTION

Aided by chaperones and other activities, secretory proteins fold precisely to their native conformations as they transit through the endoplasmic reticulum (ER). However, cells can encounter conditions during which demand on ER protein-folding activities exceeds capacity. During these instances of "ER stress" unfolded proteins accumulate within the organelle, triggering intracellular signaling pathways collectively called the unfolded protein response (UPR). The UPR transcriptionally upregulates genes encoding chaperones, oxidoreductases, and ER-associated degradation (ERAD) components (Travers et al., 2000). In metazoans, the UPR also transiently inhibits translation (Harding et al., 2002; Zhang and Kaufman, 2006). Thus, UPR outputs are adaptive because they reduce secretory protein load, enhance protein-folding capacity and promote degradation of misfolded proteins (Brodsky and McCracken,

*Correspondence: frpapa@medicine.ucsf.edu (F.R.P.).

1999; Meusser et al., 2005; Ron and Walter, 2007). In mammalian cells, the UPR can also trigger apoptosis, perhaps when adaptive outputs fail (Zhang and Kaufman, 2006).

Cells are described as experiencing "ER stress" if they have induced downstream UPR components, such as the ER chaperone BiP. But this operational definition is circular, and it is easy to see that the definition breaks down when the UPR machinery is disabled or absent. Cells lacking UPR components are likely to be more stressed than their wild-type counterparts as they are unable to effectively mount a response. Conversely, UPR activation indicates that a response has been initiated, but not whether homeostasis becomes restored. Unfolded proteins are likely to be the UPR's activating input signals (Credle et al., 2005; Kimata et al., 2007; Zhou et al., 2006), but it is difficult to measure unfolded proteins in organelles even with disruptive techniques, and unfeasible to measure them directly within living cells. However, measuring UPR activity in living cells using transcriptionally-activated fluorescent protein reporters is straightforward (Back et al., 2006; Iwawaki et al., 2004; Travers et al., 2000). If a gauge could be developed to also measure changes in ER protein-folding functions under stress, it should reveal how far such functions drift from homeostasis when perturbed, and indicate whether the UPR successfully promotes adaptation, thereby providing a more comprehensive picture of the physiological state of ER protein folding in living cells.

The ER's molecular environment is specialized to fold secretory proteins. Compared to the cytosol, the ER has greater calcium concentration, a more oxidizing redox potential, and dedicated enzymes for protein glycosylation (van Anken and Braakman, 2005). Distinct stresses ensue when the activities supporting these specialized functions are focally perturbed, either genetically or pharmacologically. But if ER functions are tightly coupled, a focal stress such as ER calcium depletion, for example, could ripple outward to provoke other stresses, such as decreased protein glycosylation. Such ripple effects might occur if glycosylating enzymes function best in a calcium-rich environment. If true, we reasoned that it should be possible to gather global information about changes in ER protein-folding capacity through measuring effects of different stresses on a single ER function. To this end, we decided to measure changes in the ER's redox potential as protein folding is perturbed.

The ER maintains an oxidizing redox potential to promote disulfide bond formation in maturing secretory proteins (Sevier and Kaiser, 2002; Tu and Weissman, 2004). Under "ER stress" the UPR upregulates catalytic activities to further enhance disulfide bond formation and promote oxidative protein folding (Travers et al., 2000). However, an overwhelming secretory protein load could saturate the ER's oxidative folding machinery, which should impede disulfide bond formation and folding of many ER-localized proteins. So depending on the strength and timing of adaptive responses, the ER's redox environment may deviate from its set point in either direction as unfolded proteins accumulate. An ER redox gauge should therefore report widely on different stresses. To test this concept, we adapted fluorescent proteins to monitor ER redox status and UPR activity dynamically in populations of single cells under stress.

RESULTS

Characterization of an ER-localized redox-sensing GFP

To follow the ER's redox state *in vivo*, we adapted recently described redox-sensitive green fluorescent proteins (GFP) as oxidation reporters for the ER (Dooley et al., 2004; Hanson et al., 2004). These GFPs have an engineered cysteine pair on adjacent surface-exposed β-strands that become disulfide-linked under oxidizing conditions. Disulfide formation reorients GFP's chromophore, altering fluorescence excitability from two maxima: 400 and 490 nm. When oxidized, excitation from 400 nm increases, while excitation from 490 nm decreases; when reduced the opposite trend occurs. Therefore, the ratio of fluorescence excitation from these two wavelengths provides an internally-controlled readout of this GFP's redox state, while

canceling out factors affecting absolute optical sensitivity (e.g. varying fluorescence output due to photobleaching, changes in reporter levels, etc.).

We appended the ER retrieval signal, HDEL, to the C-terminus of a variant called roGFP2 for ER expression. The recombinant tagged protein called eroGFP (ER-targeted redox-sensitive GFP) displayed distinct excitation spectra in the fully oxidized and reduced species, with maxima at 400 and 490 nm (Figure 1A). Titration with increasing concentrations of reduced to oxidized lipoic acid caused fluorescence emission from 400 nm excitation to incrementally decrease and emission from 490 nm excitation to increase. The curves intersected at an isosbestic point indicating two equilibrating species (Figure 1B). The ratio of fluorescence from these two excitation maxima could be related back to the fraction of reduced eroGFP. Fitting a curve to the reduced eroGFP fraction gave a midpoint value of −282 +/−3mV (Figure 1C).

DNA sequences encoding the cleavable signal peptide of the ER chaperone Kar2p were N-terminally fused to eroGFP's coding sequence, and the reporter was expressed in *S. cerevisiae*. eroGFP co-localized with the ER marker Sec61p, indicating proper ER targeting (Figure 1D). To monitor eroGFP *in vivo*, we used flow cytometry to measure the ratio of fluorescence from excitation at 488 nm versus 405 nm. This ratio—expressed in log_2 space and normalized to wild-type untreated cells—is called the "eroGFP ratio". Cells treated with increasing dithiothreitol (DTT), a cell-permeable reductant, displayed progressively increasing eroGFP ratios that saturated when the reporter was completely reduced (Figure 1E). The eroGFP ratio of a cysteine mutant (C147S) unable to form the surface disulfide did not increase with DTT (Figure S1A). The oxidant H_2O_2 caused only a slight decrease in the eroGFP ratio, allowing us to estimate that eroGFP is 96.9% oxidized (+/−0.3% SD) *in vivo* (Figure 1E).

To use eroGFP as an ER stress reporter, we first needed to ensure that it did not affect UPR signaling. Expression of eroGFP did not provoke *HAC1* mRNA splicing (Figure 1F, lanes 1 vs. 3), which occurs under ER stress (Cox and Walter, 1996; Kawahara et al., 1997). Cells treated with the ER stress-inducing agent tunicamycin (Tm) displayed comparable *HAC1* splicing with or without eroGFP expression (Figure 1F, lanes 2 vs. 4). Therefore eroGFP neither perturbs ER function to activate the UPR, nor does it compromise the UPR's ability to signal when unfolded proteins accumulate.

Dynamic monitoring of ER redox changes and UPR activity during pharmacologically-induced ER stress

To monitor the UPR, we constructed a second reporter gene encoding the red fluorescent protein, mCherry, driven by a minimal CYC1 promoter and four tandem unfolded protein response elements that the UPR transcription factor Hac1p binds—we call this UPR-RFP. eroGFP and UPR-RFP genes were combined onto a single construct that was chromosomally integrated (Figure 2A). For dynamic monitoring, we employed an automated setup recently developed by Chin and colleagues to inject 10^4–10^5 cells growing in bioreactors into a flow cytometer every 3–10 minutes over 3–14 hours (Chin et al., 2008). A combination of 3 laser lines allowed measurement of the eroGFP ratio and UPR-RFP level of individual cells as they passed through the flow cytometer (Figure 2B). Through the automated setup, single cells within large populations could be interrogated in these two metrics, and the populations represented as time-lapse histograms as ER-stress agents were added or removed (Figures 2C–F).

DTT unfolds ER proteins by reducing disulfides, thereby activating the UPR. In wild-type cells, DTT caused a rapid increase in the eroGFP ratio, apparent on the histogram as a deflection of the entire population (Figure 2C). Resolved on a finer time scale, the median eroGFP ratio deflected within 3 minutes, peaking to 1.5 by 12 minutes (Figure S2). The upward spike was

followed by a steady decline over many hours (Figure 2C). Media exchange experiments showed that this decline was due in part to cellular adaptation, rather than just DTT oxidation (Figure S3). Changes in eroGFP ratio were not due to re-localization, since the reporter remained co-localized with Sec61p during DTT treatment (Figure S4).

The UPR-RFP metric (defined as fluorescence from 532nm excitation, expressed in log_2 space, and normalized to wild-type untreated cells) started to deflect 40 minutes after DTT addition, and steadily increased from 0 to 5 over ten hours (Figure 2D). During this time course, we witnessed induction and accumulation of UPR target activities promoting ER protein oxidation, such as the protein-disulfide isomerase, Pdi1p, which increased within two hours and remained elevated over eight hours (Figure S5).

ER protein folding can be perturbed through a different mechanism using Tm, which inhibits protein glycosylation. If glycosylation and disulfide bond formation in the ER are interlinked, Tm could cause under-oxidation of ER proteins. Alternatively, UPR activation by Tm could cause ER hyperoxidation as oxidoreductases become upregulated. eroGFP ratios in the entire population of cells treated with Tm steadily increased, clearly indicating reduction of the reporter (Figure 2E). Unlike rapid changes from DTT, the eroGFP ratio of Tm-treated cells started to deflect 60 minutes after treatment, progressively increasing over four more hours up to 0.75. As with DTT, eroGFP remained ER-localized after Tm treatment (Figure S4). As with DTT, Tm caused UPR-RFP to increase from 0 to 5, albeit with a 70 minute lag time because Tm affects folding of newly synthesized ER proteins, while DTT also unfolds existing ones (Figure 2F). Movie S1 and Movie S2 show that while dynamic changes in the UPR-RFP metric were remarkably similar for both treatments, dynamic eroGFP ratio changes were very distinct.

To confirm that changes in the eroGFP ratio reflected changes in its oxidation state *in vivo*, we incubated extracts from cells treated with DTT or Tm with the thiol-alkylating agent AMS. Non-reducing gels showed only one slower migrating form of eroGFP after DTT treatment, suggesting that its disulfide had been completely reduced, and thereafter AMS modified (Figure 2G, lanes 1 and 2). Tm treatment produced both oxidized (disulfide-protected) and reduced (AMS-modified) species, consistent with its intermediate eroGFP ratio (lane 3). The control eroGFP (C147S) could be AMS-modified with or without ER stress-inducing agents (Figure S1B).

The lag time needed to change the eroGFP ratio under Tm suggested that eroGFP oxidation changes were secondary to glycosylation inhibition of proteins promoting disulfide bond formation. To test this notion, we incubated yeast extracts with AMS after treatment with DTT or Tm, and immunoblotted for the ER oxidase, Ero1p (Frand and Kaiser, 1998; Pollard et al., 1998). Ero1p is a glycoprotein and Tm treatment caused complete underglycosylation *in vivo*. DTT treatment produced a single AMS-modified (slower migrating) species, indicating complete reduction of Ero1p. Tm caused intermediately-migrating AMS-modified Ero1p species, indicating incomplete oxidation (Figure S6). As Ero1p is the proximal generator of oxidizing equivalents necessary for forming disulfide bonds in the ER, its incomplete oxidation could be expected to impair its ability to oxidize other ER proteins such as eroGFP.

Another possibility could explain the lag time for eroGFP reduction under Tm treatment: reduced eroGFPs may represent newly-synthesized proteins unable to form disulfides during glycosylation inhibition. To address this, we positioned eroGFP under the inducible GAL1 promoter, so we could rapidly terminate its expression with glucose. Pulse-chase analysis confirmed that eroGFP synthesis ceased after glucose addition (Figure S7A). Since eroGFP decayed with a 4 hr half-life (Figure S7B), it provided a long time window to monitor its fluorescence. As with cells continually synthesizing eroGFP (SGal), cells switched to glucose (SD) experienced similar increases in eroGFP ratio with DTT or Tm (Figure S7C–F). These

results indicated that eroGFP oxidation changes under stress do not result merely from an inability to form disulfides in newly imported eroGFP, but must also include reduction of pre-existing eroGFP.

ER redox changes are affected by genetic background

Since the eroGFP ratio of cells exposed to DTT declined while UPR-RFP rose (Figures 2C and D), UPR activity may have been re-oxidizing ER proteins after DTT treatment. To test this genetically, we integrated our composite reporter into deletion mutants of two UPR genes —*IRE* and *HAC1*—needed to sense and respond to unfolded proteins (Cox et al., 1993; Cox and Walter, 1996). As with wild-type cells (Figure 2C–F), the UPR mutants displayed unimodal distributions in both eroGFP ratio and UPR-RFP metric under treatment (not shown); therefore their medians were informative of the whole population, and are henceforth presented as overlaid trajectories instead of histograms (Figure 3). Unexpectedly, the resting median eroGFP ratio of both UPR mutants was identical to wild-type (i.e at 0), indicating that protein oxidation was preserved under unstressed conditions to the extent that eroGFP could be fully oxidized.

However, when challenged with DTT, both UPR mutants exhibited greater eroGFP ratio increases than wild-type, peaking to 2 by twenty minutes (Figures 3C and E), and remaining elevated throughout the time course in contrast to the steady decay seen in wild-type cells (Figure 3A). Tm also caused greater eroGFP ratio changes in the UPR mutants than in wild-type, peaking to 1.5 (Figure 3B,D, F). The UPR-RFP metric was initially -3 for *ire1*Δ and -2 for *hac1*Δ, and exhibited only a slight upward drift under DTT or Tm, which may have occurred due to RFP accumulation in the cells as they became growth arrested (see analysis below).

To ask whether re-oxidation occurs after glycosylation stress is relieved, we diluted wild-type cells treated with Tm for four hours into fresh media lacking Tm, and found that the eroGFP ratio steadily decreased over eight more hours. The UPR-RFP metric remained elevated for three hours after dilution, after which it also descended back towards its initial state as the population resumed growth (Figure S8). In contrast, the eroGFP ratio in both UPR mutants remained elevated upon Tm washout, and the mutants did not resume growth (Figure S8). Taken together, these results implied that the UPR is needed to both buffer the ER against acute challenges to oxidative folding, and to re-establish homeostasis after stress is encountered.

Since UPR transcriptional targets include enzymes mediating ER protein oxidation, we next measured the behavior of mutants in two ER oxidation genes—*ERO1* and *PDI1*—to DTT and Tm. These genes encode enzymes that generate disulfide bonds in secretory proteins through a relay of dithiol-disulfide exchange reactions (Sevier and Kaiser, 2002; Tu and Weissman, 2004). As both genes are essential, we expressed our composite reporter in DAmP alleles for *PDI1* and *ERO1*, which are hypomorphic due to reduced mRNA abundance (Schuldiner et al., 2005). Unexpectedly, both mutants had a resting eroGFP ratio similar to wild-type (i.e. near 0). Compensation from elevated UPR activity may have allowed complete oxidation of eroGFP in these hypomorphs as the initial UPR-RFP metric was 2 and 1 for *pdi1*-DAmP and *ero1*-DAmP respectively (Figures 3G, H, I, and J). However, DTT treatment of these mutants caused rapid increases in the eroGFP ratio to 1.5 by 20 minutes (Figures 3G and 3I). After its initial spike, the eroGFP ratio modestly decreased, but not to the same extent as in wild-type cells. Moreover, the UPR-RFP metric only increased by 3 and 4 for *pdi1*-DAmP and *ero1*-DAmP respectively, compared to an absolute increase of 5 in wild-type (Figures 3A, G, and I).

Surprisingly, Tm treatment of these mutants caused a smaller eroGFP ratio change than in wild-type cells (Figures 3H and J). In both mutants, eroGFP displayed a maximal increase of 0.70 compared to 0.75 for wild-type cells, and remained slightly below that of wild-type

throughout the time courses. However, for both mutants changes in the UPR-RFP metric from DTT or Tm treatment were indistinguishable (Figures 3H and J).

Another critical ER function is to identify and remove misfolded secretory proteins for degradation by the 26S proteasome, a process called ERAD (Meusser et al., 2005; Romisch, 2005). To study ER oxidation changes when ERAD function is compromised, we expressed our composite reporter in a strain deleted for *HRD1*, which encodes an E3 ubiquitin ligase needed to degrade ER luminal misfolded proteins (Bays et al., 2001; Deak and Wolf, 2001). Like the protein oxidation mutants, *hrd1*Δ's initial eroGFP ratio was 0. Its initial UPR metric was also elevated at 2 (Figures 3K and L). In *hrd1*Δ, DTT caused the eroGFP ratio to increase to 1.3 over the first 20 minutes, after which it leveled off to 0.75 with a slower decay than in wild-type (Figure 3K). Under Tm, the eroGFP ratio rose to 0.8—also slightly greater than wild-type (Figure 3L). Rises in the UPR-RFP metric of *hrd1*Δ cells were indistinguishable under DTT or Tm treatment (Figure 3L).

Redox deviations occur under conditions of physiological ER stress

Until now, we have only employed chemical agents to induce extreme and non-physiological ER protein misfolding. We next inquired whether ER oxidation changes occur during physiologically-relevant challenges such as inositol starvation, a stress known to activate the UPR (Cox et al., 1997; Nikawa and Yamashita, 1992). To this end, we removed inositol from the media of dividing wild-type cells. The UPR-RFP metric began to rise 140 minutes after inositol starvation, increasing to 2 before slightly decreasing, then leveling off (Figure 4B). This decline to a lower sustained level could be due to a slight overshoot in UPR signaling, or could indicate a fine tuning of the response as it established homeostasis. However, the eroGFP ratio remained unchanged at zero over the ten hour starvation (Figure 4A). This suggested that UPR induction may have consequently protected the ER from under-oxidation. To test this idea, we repeated the inositol starvation experiment in *ire1*Δ and *hac1*Δ mutants. As expected, the UPR-RFP metric was initially -3 for *ire1*Δ and -2 for *hac1*Δ, and drifted upward due to RFP accumulation (Figures 4D and 4F). Strikingly, two subpopulations with different eroGFP ratios emerged at 4.5 hours after inositol starvation: a deflected population and a static population (Figures 4C, E and Movie S3). The deflected subpopulations had eroGFP increases of 1.3 and 1.4 and represented 51% and 69% of cells for *ire1*Δ and *hac1*Δ respectively.

As UPR mutant cells continue to grow and divide for several generations after inositol deprivation (albeit at slower rates than wild-type) (Figure 4G), we hypothesized that the distinct eroGFP populations could represent mother and daughter cells. To investigate this, we subjected eroGFP-expressing *hac1*Δ cells to a lineage-tracing strategy that fluorescently labels mother cell walls with a Cy5 dye (Chin et al., 2008). When deprived of inositol, the sub-population with the increased eroGFP ratio was clearly overrepresented as Cy5-surface stained cells (mothers), and the sub-population that maintained eroGFP in an oxidized state was underrepresented as Cy5-surface stained cells (daughters) (Figures 4H–L and Movie S4).

We next simulated another common physiological ER challenge: increased expression of secretory proteins. For this purpose, we employed different versions of the well-studied secretory protein carboxypeptidase Y (CPY). We first generated constructs expressing CPY, or the misfolded ERAD substrate (CPY*), under conditional control of the CUP1 promoter. Cells expressing P_{CUP1}-CPY or P_{CUP1}-CPY* could be induced to produce protein by adding copper sulfate ($CuSO_4$) (Figure S9B). $CuSO_4$ addition to cells harboring empty vector caused neither eroGFP nor UPR-RFP to deflect (Figure S9A). Induction of CPY with 200μM $CuSO_4$ changed neither eroGFP ratio nor UPR-RFP metric (Figures 5A and B), but escalation of $CuSO_4$ to 500μM (which produced greater amounts of CPY protein—Figure S9C) revealed a small sub-population (3.7% of the total during the entire time course) displaying eroGFP ratios above a threshold of 1 (Figure 5I). This indicates that overexpression of an endogenous

secretory protein can cause ER oxidation changes in some cells. Induction of misfolded CPY* with 200μM $CuSO_4$ caused 5.7% of the total population to have eroGFP ratios greater than 1 (Figure 5C). This population emerged two hours after $CuSO_4$ addition, when there was 18-fold increased CPY* over baseline (Figure S9D). Dose escalation of $CuSO_4$ to 500μM further increased CPY* expression (Figure S9C), and increased the population of cells with eroGFP ratios above 1 to 12% (Figure 5K). Remarkably, the populations with increased eroGFP ratios declined near the end of the time course despite continued CPY* expression, suggesting adaptation (Figure S9D). UPR-RFP increases also became evident in these populations, and cells with greater eroGFP ratios tended to have higher UPR-RFP levels (Movie S5).

Since CPY* is efficiently degraded through ERAD, we performed two experiments to study the effects of a misfolded protein that is not efficiently degraded. First, we expressed CPY and CPY* in *hrd1*Δ cells which are compromised for CPY* degradation (Friedlander et al., 2000). Addition of 200μM $CuSO_4$ to *hrd1*Δ cells expressing CPY and CPY* caused 4.2% and 10% of the populations to have eroGFP ratios above 1 respectively (Figures 5E and G). Like wild-type, *hrd1*Δ cells that had the greatest eroGFP deflection also had the greatest increase in UPR-RFP (Figure 5H and Movie S6). Second, we expressed a non-glycosylated version of CPY*, called CPY*0000, in wild-type cells which is not efficiently degraded (Kostova and Wolf, 2005; Spear and Ng, 2005). In these cells, the percentage of cells with eroGFP ratios above 1 climbed to 16%, and deflections occurred more rapidly after $CuSO_4$ addition than with CPY* (Figure 5M). The deflected population eventually decayed, again suggesting adaptation, albeit slower than the CPY*-expressing population. (Movie S7).

Because CPY* contains 11 cysteines, we next studied the effects of eliminating the cysteines in CPY* on eroGFP changes. We generated two CUP1-inducible CPY* variants containing either 1 cysteine or no cysteines (Haynes et al., 2004). Expression of CPY*-1Cys caused similar changes as observed for CPY*, however, expression of CPY*-Cysless caused only 4.3% of cells to have eroGFP ratios above 1 (Figures 5O and Q). Thus the “potency” of CPY variants in their ability to cause eroGFP deflection was CPY*0000 > CPY* > CPY*-1Cys > CPY*-Cysless > CPY (Figure S9G).

eroGFP and UPR-RFP changes under stress reveal interlinked protein folding functions orchestrated by the UPR

While cells undergoing the relatively milder stresses of inositol deprivation or overexpression of CPY variants displayed heterogeneity in their populations, cells subjected to the strong stressors DTT and Tm deflected across both metrics as homogeneous populations. To further analyze the behavior of wild-type and mutants under these strong stresses, we displayed their eroGFP and UPR-RFP changes using trajectories in two dimensional space to illustrate two major points (Figures 6A and B). First, in the absence of stress, mutants varied in their UPR-RFP metric, yet their eroGFP ratio was the same, indicating that these mutants can sustain near complete oxidation (at least of eroGFP). Second, the two different stressors caused distinct trajectories for each strain. Only wild-type cells were capable of near complete re-oxidization of eroGFP after DTT treatment. UPR mutants displayed the greatest eroGFP deflections under both stresses, indicating their pivotal roles in countering diverse protein folding challenges. Most surprisingly, the oxidative folding mutants showed greater deflections than wild-type cells after DTT treatment, but slightly smaller changes after Tm treatment.

In all cases, UPR-RFP never decreased over the time courses. Since RFP has a long half-life and because both DTT and Tm caused growth arrest in wild-type and all mutants examined leading to its further accumulation (Figures 6C and D and data not shown), the rate of change of UPR-RFP was a better indicator of UPR activity for any given time point. To this end, we calculated the first derivative of median UPR-RFP (d(UPR-RFP)/dt) for wild-type and mutants. For wild-type cells, d(UPR-RFP)/dt was positive throughout the time course of DTT treatment,

although it declined 4 hours after treatment as eroGFP became re-oxidized (Figure 6E). For Tm treatment, d(UPR-RFP)/dt also remained positive throughout the time course, also declining before leveling off (Figure 6F). As expected, d(UPR-RFP)/dt was fixed at zero for the UPR mutants (Figures 6E and F). Surprisingly, d(UPR-RFP)/dt displayed larger maximal values in both the oxidative folding and ERAD mutants than wild-type, in Tm but not DTT (Figures 6E and F). Increased basal UPR activation in these mutants may allow for faster UPR induction under stress. Indeed, *pdi1*-DAmP displayed 28% greater *HAC1* mRNA splicing than wild-type in the absence of Tm, suggesting that it was "pre-conditioned" due to low level UPR activation. (Figure S10). As DTT unfolds existing ER proteins rapidly, while Tm affects folding of newly synthesized proteins (and therefore more slowly), differences in UPR activation kinetics may be less apparent in the former treatment than in the latter.

To quantify the stressed state further, we integrated the area under each eroGFP ratio curve (AUC) over the time course of stress for each mutant, and normalized the AUCs by subtracting from wild-type's AUC (Figure S11). Normalized this way, a positive AUC denotes greater cumulative eroGFP change over the time course than wild-type, while negative values indicated less change. A heat map of the analysis (Figure 6G) showed that ERAD and UPR mutants were uniformly more stressed than wild-type under Tm or DTT. Unexpectedly oxidative folding mutants were less stressed than wild-type during Tm, but more stressed under DTT. We therefore predicted that *ero1*-DAmP cells would grow under Tm but not DTT, and confirmed this notion (Figure S12). Interestingly, *ero1*-DAmP cells grew slightly better than wild-type in Tm, consistent with their negative AUC.

Taken together, our results show that the UPR is necessary to orchestrate readjustment of ER protein oxidation under distinct stresses. We therefore asked whether UPR activity is also sufficient to buffer ERs from under-oxidation during stress. To this end, we applied a chemical-genetic approach we previously developed to activate the UPR in the absence of stress. Through rational protein engineering, Ire1p—a bi-functional ER transmembrane kinase/RNase responsible for UPR signaling—can be sensitized to a cell-permeable nucleotide analog called 1NM-PP1. In *ire1*Δ cells harboring this Ire1 allele, 1NM-PP1 activates the UPR independent of stress (Papa et al., 2003). Treatment with 1NM-PP1 caused a slight decrease in the eroGFP ratio, suggesting hyperoxidation of the ER. Adding 1NM-PP1 and Tm together caused a smaller increase in the eroGFP ratio compared to Tm alone, suggesting a buffering effect against protein under-oxidation (Figure 6H). UPR output therefore is both necessary and sufficient to mitigate under-oxidation of ER proteins during stress.

DISCUSSION

This is the first study of "ER stress" using real-time analysis to interrogate the stressed state of single cells within large populations. We utilized separate reporters to measure two independent variables: UPR-RFP for UPR activity, and a redox-sensitive reporter—eroGFP—to follow oxidation of cysteine sulfhydryls to disulfides. Thus eroGFP was positioned as a "proximal" reporter for the critical ER function of disulfide formation. eroGFP is internally controlled because it is ratiometric by excitation, obviating the need to consider and correct for confounding factors affecting absolute reporter levels. Although an individual eroGFP molecule is either reduced or oxidized (binary), cumulative fluorescence from many eroGFP molecules provided a continuous (analog) readout of eroGFP's average oxidation state within single cells. Adding UPR-RFP as a "distal" reporter for UPR signaling provided complementary information that could not have been gathered using either reporter alone. Our design strategy of positioning proximal and distal reporters may be useful for studying other intracellular signaling pathways where input signals are not easily quantifiable.

We propose a model that accounts for our observations and analyses, and provides conceptual advances (Figure 7). Using our systems, we found (as expected) that chemical reduction is a "primary" stress causing under-oxidation of eroGFP and other ER proteins—we refer to this as ER oxidative folding stress. Unexpectedly, other challenges to protein folding—including under-glycosylation, inositol deprivation, and increased protein secretion—"secondarily" caused varying degrees of ER oxidative folding stress. Based on these results, we propose that the ER's protein folding, modification, and quality control systems are functionally interlinked with the oxidative folding machinery—and by extension perhaps with each other. Thus, eroGFP can measure many discrete challenges to ER function that have historically been grouped and studied under the rubric of "ER stress".

Our model highlights four extreme states of ER oxidation state and UPR activity. Consistent with previous estimates of a highly oxidizing ER redox potential obtained through disruptive methods (Hwang et al., 1992), eroGFP was almost completely oxidized in wild-type cells without imposed stress. Unexpectedly, eroGFP remained similarly oxidized in all mutants tested in this study. This unexpected result points to a remarkable plasticity in ER oxidative folding. Only through actively perturbing ER functions are eroGFP differences between mutants revealed. Unstressed UPR mutants can still support ER oxidation, perhaps because the UPR is only required to increase expression of ER oxidoreductases during stress. ER oxidation, however, is essential, and hypomorphs in oxidative folding activities exhibit an adapted state through low-level UPR activation.

The ER-stressed (UPR-activated) state can be achieved in any cell competent for UPR signaling. Here the combination of eroGFP and UPR-RFP revealed subtle differences between mutants under distinct stresses. Both *ero1*-DAmP and *pdi1*-DAmP resisted challenges to glycosylation better than oxidation. This difference may occur because UPR activation resets ER oxidation to minimum levels for viability, but in the process augments other ER folding activities such as those supporting glycosylation. Thus these mutants come "pre-conditioned" against challenge to other functions. We predict that many such pre-conditioned states could exist, and dynamic monitoring with eroGFP should delineate these at the genomic level, allowing assignment of primary functions to uncharacterized genes. Pre-conditioning could also be achieved through chemical-genetic activation of Ire1, which revealed slight hyperoxidation in the absence of stress. Future versions of eroGFPs exhibiting more oxidizing midpoint potentials may allow more accurate quantification of these changes under both resting and stressed states.

The ER-stressed (decompensated) state of UPR mutants was revealed through larger and sustained eroGFP deflections than wild-type under stress, and could not have been described using the distal UPR-RFP reporter alone. Therefore measuring eroGFP oxidation changes provides information on drift from ER homeostasis, while measuring UPR activity provides information on compensation.

How can eroGFP become reduced during myriad ER stresses? Like any ER protein containing cysteines, eroGFP must be oxidized through dithiol-disulfide exchange reactions through specific protein-protein interactions mediated by oxidoreductases. These activities may become compromised during stress. Indeed, oxidation of Ero1p decreased when under-glycosylated. Additionally, as the vast majority of secretory proteins contain cysteines, their accumulation in unfolded form may saturate the ER's oxidative machinery due to futile cycling attempts to form disulfide bonds (Haynes et al., 2004). This effect may occur in some cells during overexpression of the cysteine-containing protein, CPY and its misfolded variants. Interestingly, overexpression of a cysteine-less CPY* variant still caused eroGFP deflection in some cells (although to a lesser degree than a variant containing one cysteine) indicating that a saturation mechanism cannot be the sole explanation for eroGFP changes.

Because we also observed reduction of pre-existing eroGFP, its disulfide bond must be labile and may become reduced by enzymatic activities or ER permeable reductants such as glutathione. PDI has been shown to have reductase activity, facilitating removal of unfolded proteins from the ER (Tsai et al., 2001). More recently a mammalian ER reductase, ERdj5, was described (Ushioda et al., 2008). Interestingly, a conserved disulfide in the ER-luminal domain of the UPR sensor ATF6 is reduced during ER stress, allowing ATF6 to traffic to the Golgi for processing and activation (Nadanaka et al., 2006). When protein oxidation becomes generally compromised during ER stress as we have shown, ATF6's labile disulfide bond may become reduced, raising the exciting prospect that ER homeostasis is maintained through sensing both redox state as well as unfolded proteins.

While we observed eroGFP co-localized with the ER (i.e. in reticular structures containing Sec61) during stresses we imposed, it is conceivable that dynamic remodeling of ER to terminal or salvage organelles may expose eroGFP to less oxidizing milieus, also contributing to its reduction.

Finally, eroGFP revealed unanticipated heterogeneities between individual cells in a number of our experiments. During inositol starvation, the eroGFP ratio rose in UPR-deficient mother cells, but not in daughters. We speculate that asymmetric segregation of ER tubules containing under-oxidized proteins may occur under stress. This observation adds to reports that oxidatively damaged cytosolic and mitochondrial proteins are retained in mothers (Aguilaniu et al., 2003). The heterogeneity observed for CPY* expression—which could represent a stress to which cells can successfully adapt—also suggests that some individuals escape homeostatic control. Such differences may account for different cell fate outcomes in metazoans, which eliminate highly stressed cells through apoptosis. The metazoan UPR can alternatively transmit survival or apoptotic signals though it is unclear how the UPR separates and relegates some cells to an apoptotic fate, while allowing others to successfully adapt. The tools and concepts we have developed may be applicable to the study and understanding of such questions.

EXPERIMENTAL PROCEDURES

Plasmid Construction

See Supplemental Experimental Procedures

Determination of redox midpoint potentials

1μM recombinant eroGFP was diluted into buffer containing 75mM HEPES (pH 7.0), 140mM NaCl, 1mM EDTA, and 10mM total lipoic acid in an anaerobic glove box for one hour at 21.5 C. The lipoic acid consisted of a mixture of oxidized and reduced species that ranged from 10mM reduced to 10mM oxidized in 1mM increments. Fluorescence spectra were measured on a Spectramax M2 microplate reader (Molecular Devices) with excitation wavelengths from 350nm to 500nm with a 2nm step and emission wavelength at 520nm. Midpoint determination was performed as described (Hanson et al., 2004) and plots were made with Origin software.

Media and strains

Strains were from the Yeast Consortium Deletion Library (Giaever et al., 2002) or from the DAmP library (Schuldiner et al., 2005) (Table S1). Sec61-mCherry yeast were a gift from Bernales, S and Walter, P (Bernales et al., 2006). Cultures were grown in SD or SGal complete media supplemented with myo-inositol (Sigma) at 100μg/ml. For flow cytometry time courses, DTT (Roche) was 2mM and Tm (CalBiochem) was 1ug/ml. For inositol starvation experiments, cells were washed twice with pre-warmed sterile water and resuspended into pre-warmed SD complete media lacking inositol. Cell surface Cy5 labeling was previously

described (Chin et al., 2008). All CPY* experiments used SD-leucine+inositol media to maintain plasmid selection.

Light Microscopy

Exponentially growing cells were imaged with a Yokogawa CSU-22 spinning disc confocal on a NikonTE2000 microscope. The images were recorded with a 100x / 1.4 NA Plan Apo objective on a Cascade II EMCCD with a sample magnification of 60nm/pixel. eroGFP was excited with the 488nm Ar-ion laser line and Sec61-mCherry was excited with the 568 nm Ar-Kr laser line. Micro-Manager and ImageJ were used to control the microscope and process the images.

Northern Blot Analysis

Northern blots were previously described (Papa et al., 2003).

Flow Cytometry Analysis

Fluorescence was measured with a flow cytometer (LSRII, BD) with a setup described in Figure 2B. Cell delivery to the cytometer was automated as described (Chin et al., 2008). Data analysis was performed using MATLAB (The Mathworks). eroGFP and UPR-RFP values for each mutant were normalized to wild-type and corrected based on their baseline values (data not shown). The first derivative of UPR-RFP at time t,

$$\frac{d(\mathrm{UPR-RFP})}{\mathrm{dt}} = \frac{\mathrm{UPR-RFP}(t+\Delta t) - \mathrm{UPR-RFP}(\Delta t)}{\Delta t}$$

was calculated as the difference in UPR-RFP form two consecutive time points t and t+Δt, divided by the time interval, Δt = 7 minutes.

Determination of oxidation state of eroGFP and Ero1p

Oxidation state determination was performed as described (Frand and Kaiser, 1999). See supplemental experimental procedures for details.

Immunoblots

Immunoblots were performed as described (Papa et al., 2003). See supplemental experimental procedures for details.

Supplementary Material

Refer to Web version on PubMed Central for supplementary material.

ACKNOWLEDGEMENTS

We thank S. James Remington for providing the roGFP2 construct, Victor Chubukov for assistance with automated flow cytometry and for data analysis software, Maya Schuldiner, Martin Jonikas, Erin Quan, Davis Ng, and Antony Cooper for reagents, and Kurt Thorn for imaging assistance. We thank Mark Hochstrasser, Scott Oakes, Chris Patil, Jonathan Weissman, and members of the Papa lab for comments on the manuscript. Microscopy images were collected at the Nikon Imaging Center at UCSF/QB3. F.R.P. is funded through an NIH Director's New Innovator Award (DP2OD001925), a Burroughs Wellcome Fund Career Award in Biomedical Sciences, a Culpeper Scholarship from the Partnership for Cures, and startup awards from the Sandler Foundation and the Hillblom Foundation. P.I.M. is supported through a National Science Foundation Pre-doctoral Fellowship.

REFERENCES

Aguilaniu H, Gustafsson L, Rigoulet M, Nystrom T. Asymmetric inheritance of oxidatively damaged proteins during cytokinesis. Science 2003;299:1751–1753. [PubMed: 12610228]

Back SH, Lee K, Vink E, Kaufman RJ. Cytoplasmic IRE1alpha-mediated XBP1 mRNA splicing in the absence of nuclear processing and endoplasmic reticulum stress. J Biol Chem 2006;281:18691–18706. [PubMed: 16644724]

Bays NW, Gardner RG, Seelig LP, Joazeiro CA, Hampton RY. Hrd1p/Der3p is a membrane-anchored ubiquitin ligase required for ER-associated degradation. Nat Cell Biol 2001;3:24–29. [PubMed: 11146622]

Bernales S, McDonald KL, Walter P. Autophagy counterbalances endoplasmic reticulum expansion during the unfolded protein response. PLoS Biol 2006;4:e423. [PubMed: 17132049]

Brodsky JL, McCracken AA. ER protein quality control and proteasome-mediated protein degradation. Seminars in Cell and Developmental Biology 1999;10:507–513. [PubMed: 10597633]

Chin CS, Chubukov V, Jolly ER, DeRisi J, Li H. Dynamics and design principles of a basic regulatory architecture controlling metabolic pathways. PLoS Biol 2008;6:e146. [PubMed: 18563967]

Cox JS, Chapman RE, Walter P. The unfolded protein response coordinates the production of endoplasmic reticulum protein and endoplasmic reticulum membrane. Mol Biol Cell 1997;8:1805–1814. [PubMed: 9307975]

Cox JS, Shamu CE, Walter P. Transcriptional induction of genes encoding endoplasmic reticulum resident proteins requires a transmembrane protein kinase. Cell 1993;73:1197–1206. [PubMed: 8513503]

Cox JS, Walter P. A novel mechanism for regulating activity of a transcription factor that controls the unfolded protein response. Cell 1996;87:391–404. [PubMed: 8898193]

Credle JJ, Finer-Moore JS, Papa FR, Stroud RM, Walter P. On the mechanism of sensing unfolded protein in the endoplasmic reticulum. Proc Natl Acad Sci U S A 2005;102:18773–18784. [PubMed: 16365312]

Deak PM, Wolf DH. Membrane topology and function of Der3/Hrd1p as a ubiquitin-protein ligase (E3) involved in endoplasmic reticulum degradation. J Biol Chem 2001;276:10663–10669. [PubMed: 11139575]

Dooley CT, Dore TM, Hanson GT, Jackson WC, Remington SJ, Tsien RY. Imaging dynamic redox changes in mammalian cells with green fluorescent protein indicators. J Biol Chem 2004;279:22284–22293. [PubMed: 14985369]

Frand AR, Kaiser CA. The ERO1 gene of yeast is required for oxidation of protein dithiols in the endoplasmic reticulum. Mol Cell 1998;1:161–170. [PubMed: 9659913]

Frand AR, Kaiser CA. Ero1p oxidizes protein disulfide isomerase in a pathway for disulfide bond formation in the endoplasmic reticulum. Mol Cell 1999;4:469–477. [PubMed: 10549279]

Friedlander R, Jarosch E, Urban J, Volkwein C, Sommer T. A regulatory link between ER-associated protein degradation and the unfolded-protein response. Nat Cell Biol 2000;2:379–384. [PubMed: 10878801]

Giaever G, Chu AM, Ni L, Connelly C, Riles L, Veronneau S, Dow S, Lucau-Danila A, Anderson K, Andre B, et al. Functional profiling of the Saccharomyces cerevisiae genome. Nature 2002;418:387–391. [PubMed: 12140549]

Hanson GT, Aggeler R, Oglesbee D, Cannon M, Capaldi RA, Tsien RY, Remington SJ. Investigating mitochondrial redox potential with redox-ensitive green fluorescent protein indicators. J Biol Chem 2004;279:13044–13053. [PubMed: 14722062]

Harding HP, Calfon M, Urano F, Novoa I, Ron D. Transcriptional and translational control in the Mammalian unfolded protein response. Annu Rev Cell Dev Biol 2002;18:575–599. [PubMed: 12142265]

Haynes CM, Titus EA, Cooper AA. Degradation of misfolded proteins prevents ER-derived oxidative stress and cell death. Mol Cell 2004;15:767–776. [PubMed: 15350220]

Hwang C, Sinskey AJ, Lodish HF. Oxidized redox state of glutathione in the endoplasmic reticulum. Science 1992;257:1496–1502. [PubMed: 1523409]

Iwawaki T, Akai R, Kohno K, Miura M. A transgenic mouse model for monitoring endoplasmic reticulum stress. Nat Med 2004;10:98–102. [PubMed: 14702639]

Kawahara T, Yanagi H, Yura T, Mori K. Endoplasmic reticulum stress-induced mRNA splicing permits synthesis of transcription factor Hac1p/Ern4p that activates the unfolded protein response. Mol Biol Cell 1997;8:1845–1862. [PubMed: 9348528]

Kimata Y, Ishiwata-Kimata Y, Ito T, Hirata A, Suzuki T, Oikawa D, Takeuchi M, Kohno K. Two regulatory steps of ER-stress sensor Ire1 involving its cluster formation and interaction with unfolded proteins. J Cell Biol 2007;179:75–86. [PubMed: 17923530]

Kostovaz Z, Wolf DH. Importance of carbohydrate positioning in the recognition of mutated CPY for ER-associated degradation. J Cell Sci 2005;118:1485–1492. [PubMed: 15769847]

Meusser B, Hirsch C, Jarosch E, Sommer T. ERAD: the long road to destruction. Nat Cell Biol 2005;7:766–772. [PubMed: 16056268]

Nadanaka S, Okada T, Yoshida H, Mori K. A Role of Disulfide Bridges Formed in the Lumenal Domain of ATF6 in Sensing Endoplasmic Reticulum Stress. Mol Cell Biol. 2006

Nikawa J, Yamashita S. IRE1 encodes a putative protein kinase containing a membrane-spanning domain and is required for inositol phototrophy in Saccharomyces cerevisiae. Mol Microbiol 1992;6:1441–1446. [PubMed: 1625574]

Papa FR, Zhang C, Shokat K, Walter P. Bypassing a kinase activity with an ATP-competitive drug. Science 2003;302:1533–1537. [PubMed: 14564015]

Pollard MG, Travers KJ, Weissman JS. Ero1p: a novel and ubiquitous protein with an essential role in oxidative protein folding in the endoplasmic reticulum. Mol Cell 1998;1:171–182. [PubMed: 9659914]

Romisch K. Endoplasmic reticulum-associated degradation. Annu Rev Cell Dev Biol 2005;21:435–456. [PubMed: 16212502]

Ron D, Walter P. Signal integration in the endoplasmic reticulum unfolded protein response. Nat Rev Mol Cell Biol 2007;8:519–529. [PubMed: 17565364]

Schuldiner M, Collins SR, Thompson NJ, Denic V, Bhamidipati A, Punna T, Ihmels J, Andrews B, Boone C, Greenblatt JF, et al. Exploration of the function and organization of the yeast early secretory pathway through an epistatic miniarray profile. Cell 2005;123:507–519. [PubMed: 16269340]

Sevier CS, Kaiser CA. Formation and transfer of disulphide bonds in living cells. Nat Rev Mol Cell Biol 2002;3:836–847. [PubMed: 12415301]

Spear ED, Ng DT. Single, context-specific glycans can target misfolded glycoproteins for ER-associated degradation. J Cell Biol 2005;169:73–82. [PubMed: 15809311]

Travers KJ, Patil CK, Wodicka L, Lockhart DJ, Weissman JS, Walter P. Functional and genomic analyses reveal an essential coordination between the unfolded protein response and ER-associated degradation. Cell 2000;101:249–258. [PubMed: 10847680]

Tsai B, Rodighiero C, Lencer WI, Rapoport TA. Protein disulfide isomerase acts as a redox-dependent chaperone to unfold cholera toxin. Cell 2001;104:937–948. [PubMed: 11290330]

Tu BP, Weissman JS. Oxidative protein folding in eukaryotes: mechanisms and consequences. J Cell Biol 2004;164:341–346. [PubMed: 14757749]

Ushioda R, Hoseki J, Araki K, Jansen G, Thomas DY, Nagata K. ERdj5 is required as a disulfide reductase for degradation of misfolded proteins in the ER. Science 2008;321:569–572. [PubMed: 18653895]

van Anken E, Braakman I. Versatility of the endoplasmic reticulum protein folding factory. Crit Rev Biochem Mol Biol 2005;40:191–228. [PubMed: 16126486]

Zhang K, Kaufman RJ. The unfolded protein response: a stress signaling pathway critical for health and disease. Neurology 2006;66:S102–S109. [PubMed: 16432136]

Zhou J, Liu CY, Back SH, Clark RL, Peisach D, Xu Z, Kaufman RJ. The crystal structure of human IRE1 luminal domain reveals a conserved dimerization interface required for activation of the unfolded protein response. Proc Natl Acad Sci U S A 2006;103:14343–14348. [PubMed: 16973740]

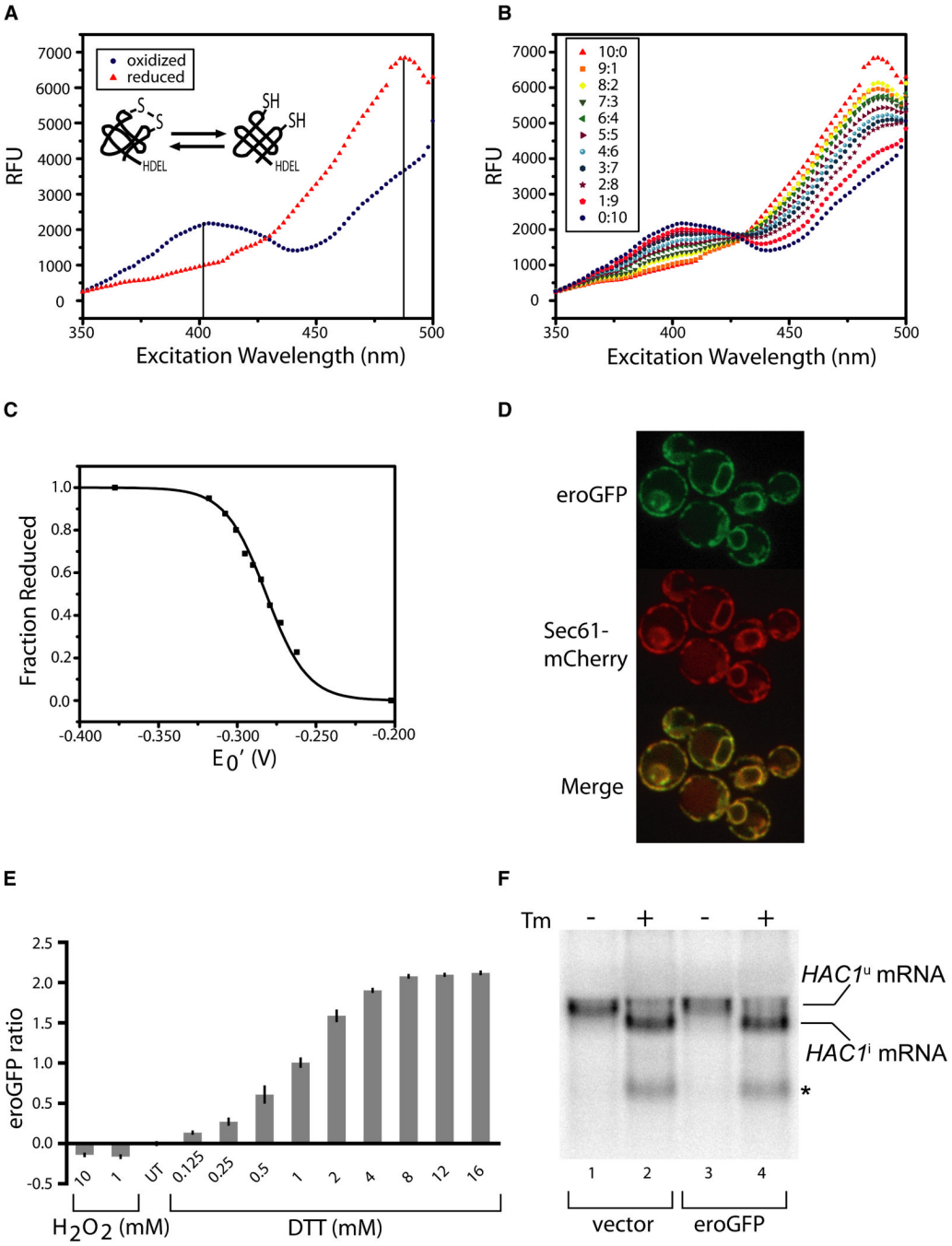

Figure 1. Characterization of an ER-localized redox-sensitive GFP (eroGFP)

(A) Fluorescence excitation spectra of recombinant fully reduced (red triangles) and oxidized (blue circles) eroGFP. Emission was measured at 520 nm. (B) Excitation spectra of recombinant eroGFP through titration of reduced to oxidized lipoic acid (ratios in inset—total 10 mM). (C) Fraction-reduced eroGFP—data from (B)—as a function of ratios of reduced to oxidized lipoic acid expressed as redox potential values. (D) Representative confocal image of cells expressing eroGFP and Sec61-mCherry. (E) eroGFP ratio (defined as the ratio of fluorescence from excitation at 488 nm vs. 405 nm expressed in $\log_2$ space and normalized to the untreated case—UT) in cells treated with the indicated concentration of DTT or H_2O_2. Data represent means +/− SD from three independent experiments. (F) Northern blot for *HAC1*

mRNA in cells expressing vector or eroGFP, treated with or without tunicamycin, Tm, (1μg/ml) for 1 hr. *HAC1*^{u} denotes unspliced and *HAC1*^{i} spliced mRNA respectively. An asterisk signifies the *HAC1* 5' exon.

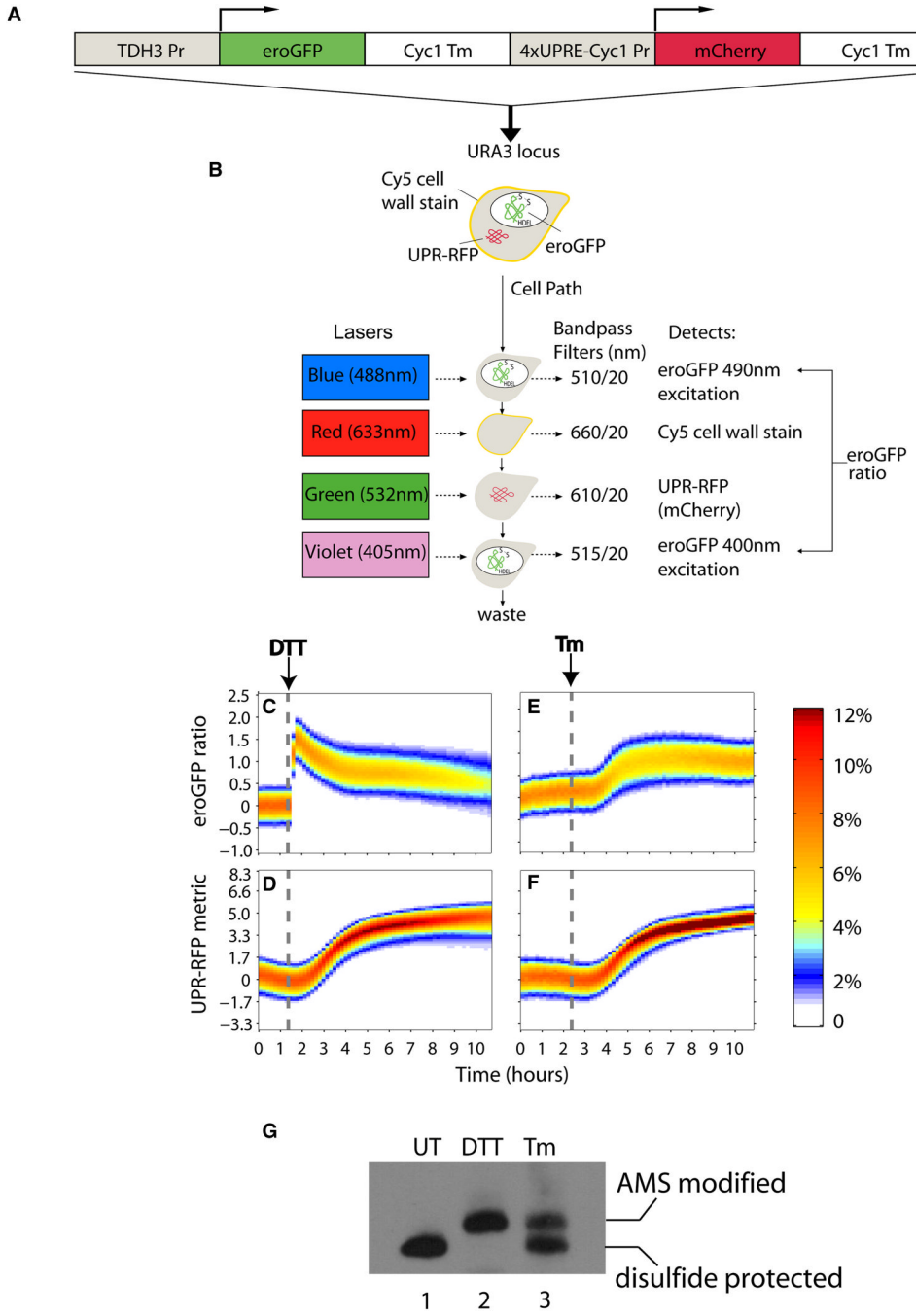

Figure 2. Dynamic monitoring of ER redox status and UPR activity during pharmacologically-induced ER stress

(A) Schematic of composite reporter gene. (B) Schematic showing configuration of flow cytometer laser lines and filters. A syringe-pump periodically (~10 minutes) injected 25µl of sample from cultures growing in bioreactors into a flow cytometer. (C–F) Time courses of eroGFP ratio or UPR-RFP metric histograms in wild-type cells during treatment with DTT (2mM) or Tm (1µg/ml). The eroGFP ratio and UPR-RFP metrics are normalized to wild-type unstressed cells. Color represents percentage of cells at a given metric value and time point. Dashed gray line signifies time of DTT or Tm addition. (G) Non-reducing SDS-PAGE and

immunoblot (anti-GFP) of AMS-treated protein extracts from untreated cells (lane 1), cells treated with 10mM DTT for 30 min (lane 2), or 2μg/ml Tm for 3 hrs (lane 3).

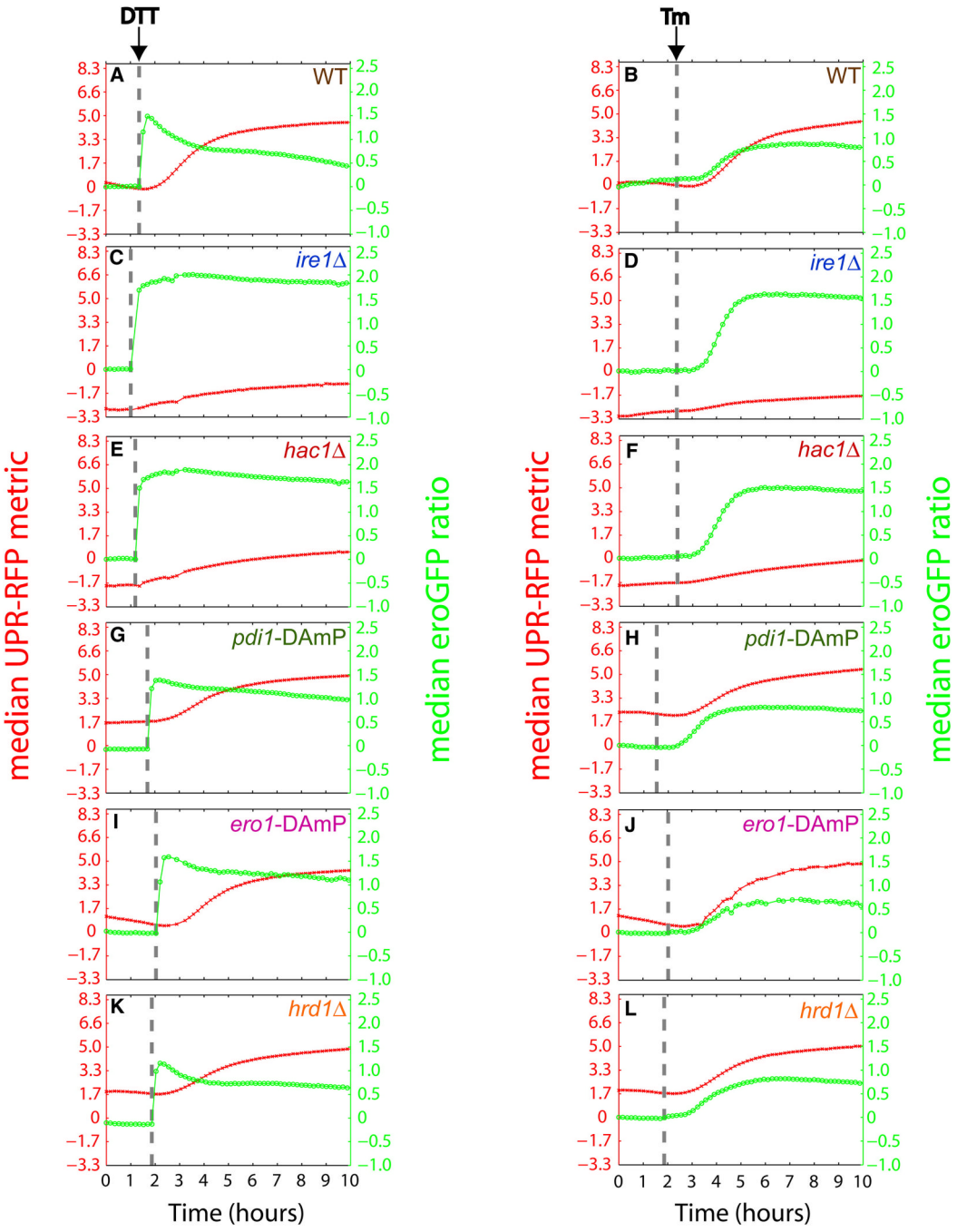

Figure 3. Dynamic monitoring of ER redox status and UPR activity in ER oxidative folding, quality control, and UPR signaling mutants during pharmacologically-induced ER stress

(A–L) Median eroGFP ratio (green circles) and UPR-RFP metric (red x-marks) during treatment with DTT (2mM) or Tm (1μg/ml) for wild-type and indicated mutants. Values are normalized to wild-type unstressed cells. Dashed gray line signifies time at which stressor was added.

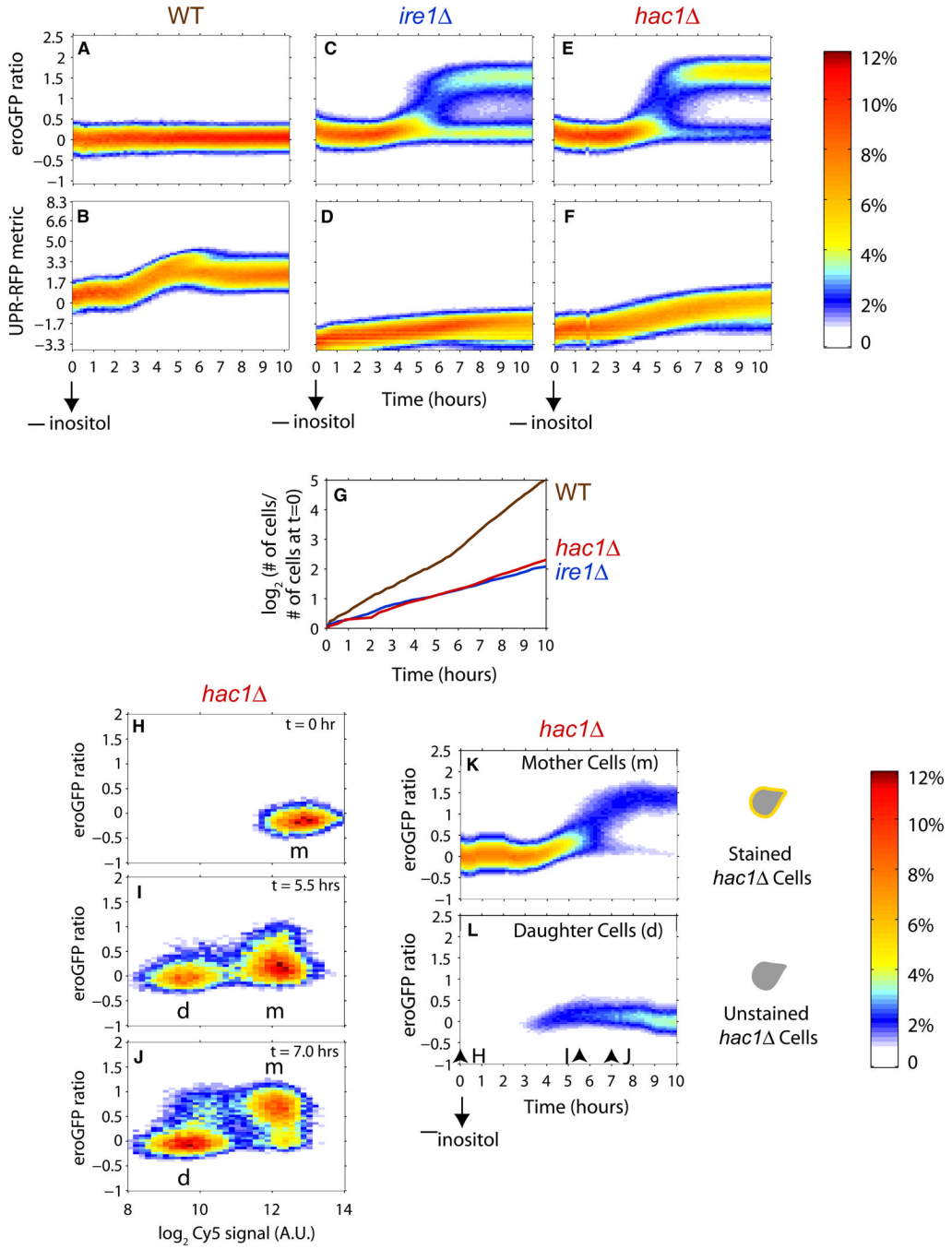

Figure 4. Dynamic monitoring of ER redox status and UPR activity during inositol starvation

(A–F) Time courses of eroGFP ratio or UPR-RFP metric histograms in wild-type, *ire1*Δ, or *hac1*Δ cells starved for inositol at time, t=0. (G) Growth curves for the time courses of (A–F). (H–J) Snapshots of *hac1*Δ cell populations for eroGFP ratio vs. Cy5 signal at three time points. Mothers (m) have a high Cy5 signal ($\log_2$ Cy5 > 10.5) while daughters (d) have a low Cy5 signal ($\log_2$ Cy5 < 10.5). Time courses of eroGFP histograms for *hac1Δ* mothers (K) and daughters (L). The three time points of (H–J) are indicated in (L). Color represents percentage of cells at a given metric value and time point.

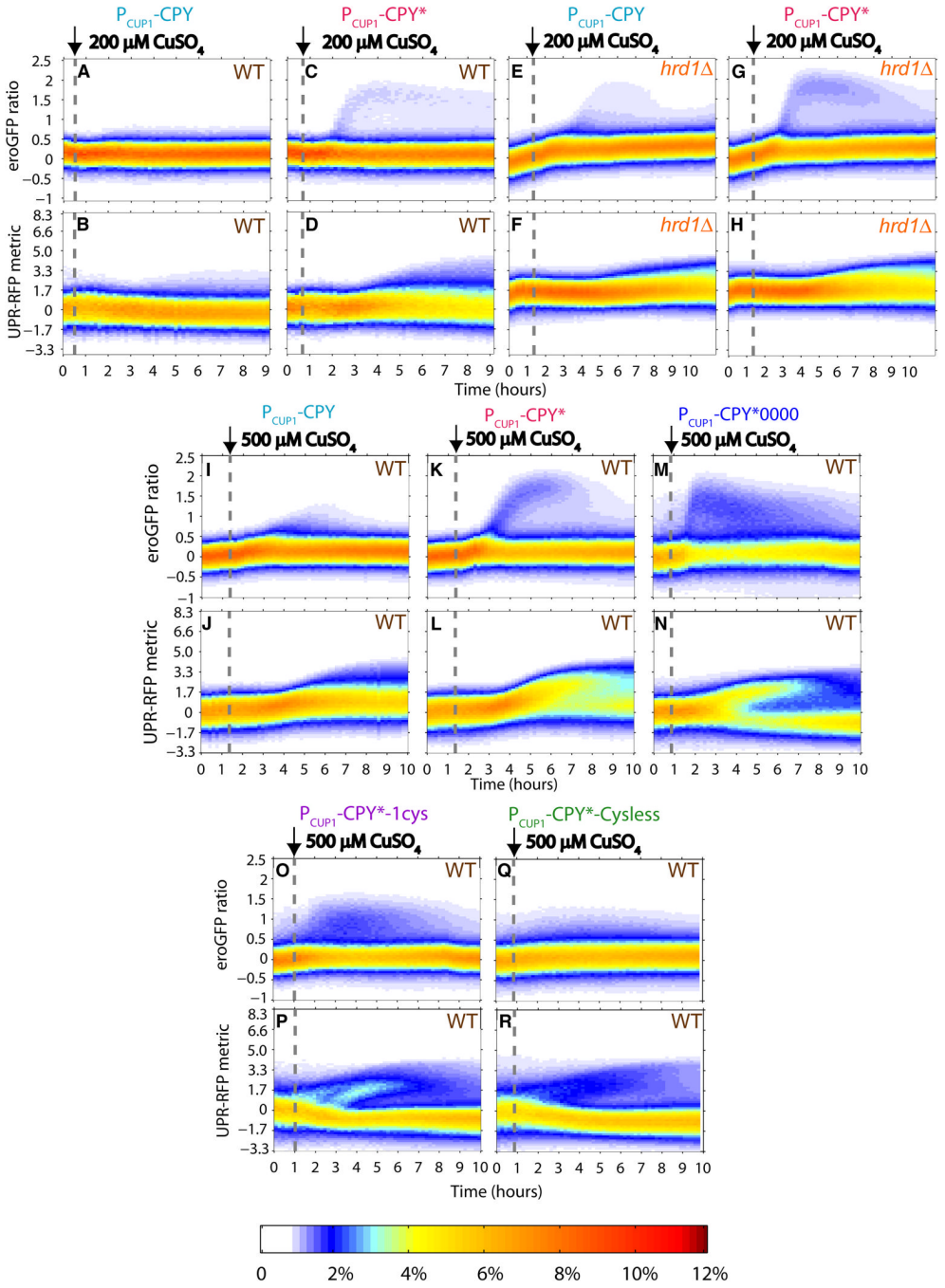

Figure 5. Dynamic monitoring of ER redox status and UPR activity during overexpression of secretory proteins

(A–R) Time courses of eroGFP ratio or UPR-RFP metric histograms in wild-type (WT) or *hrd1*Δ cells expressing CPY, CPY*, CPY*-0000, CPY*-1cys, or CPY*-Cysless under control of the copper-inducible CUP1 promoter. Color represents percentage of cells at a given metric value and time point. The dashed gray line signifies time of $CuSO_4$ (200µM or 500µM) addition.

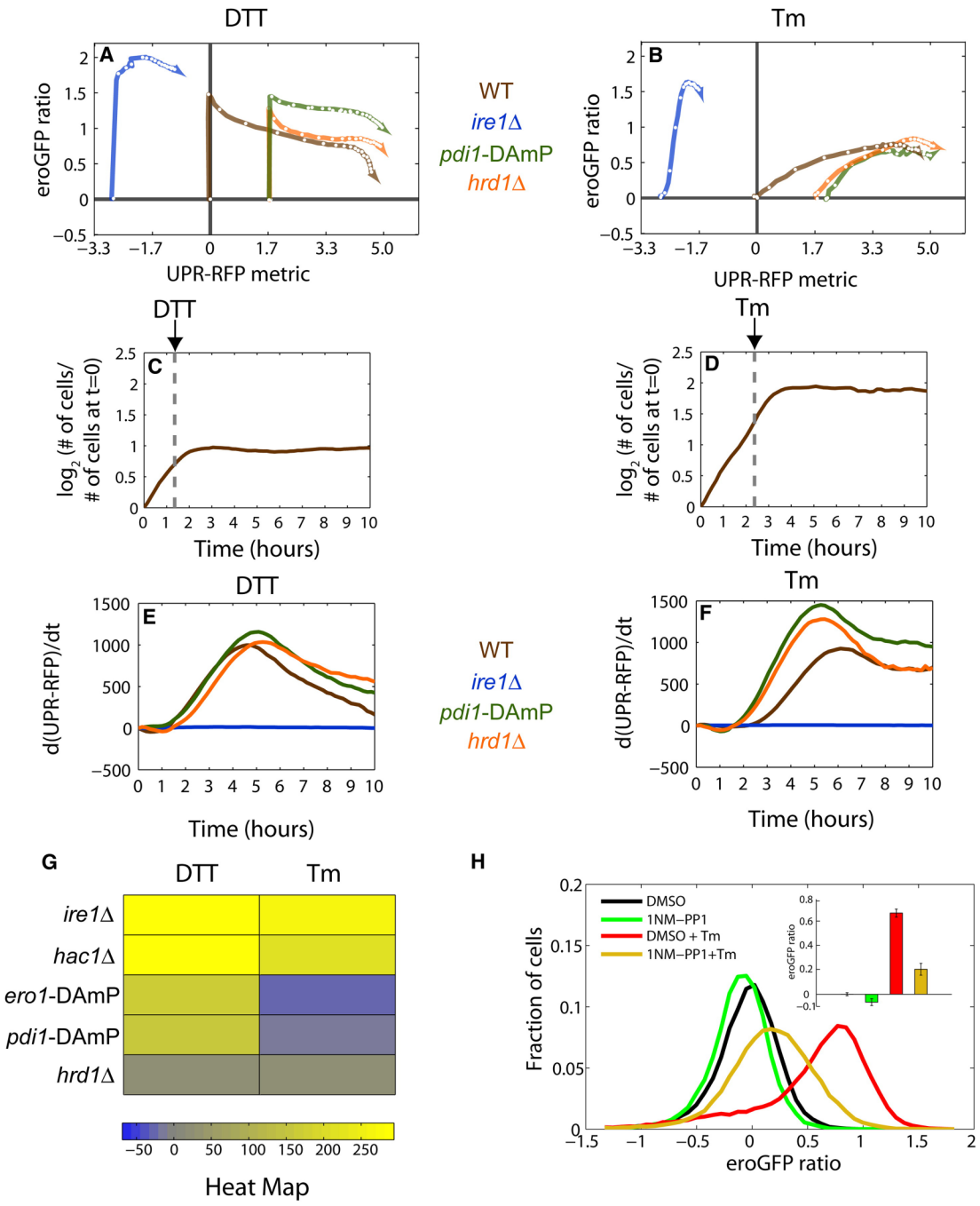

Figure 6. Analysis of ER oxidative folding, quality control, and UPR signaling mutants under stress

(A, B) Median trajectories of wild-type or mutant cells (treated with DTT or Tm) through UPR-RFP metric and eroGFP ratio two-dimensional space. The trajectories begin at the last data point before stress addition, and conclude when the time course ends (signified by the arrow). Consecutive white circles within each trajectory line are separated by 30 minutes. Color denotes each mutant. (C, D) Growth curves for wild-type cells treated with DTT (2mM) or Tm (1μg/ml). (E, F) The first derivative of median UPR-RFP with respect to time, d(UPR-RFP)/dt, vs. time for wild-type and mutants treated with DTT or Tm. (G) Integrated eroGFP ratios over the time courses for each mutant normalized to wild-type and represented as heat maps ranging from blue (negative values) to yellow (positive values). Data for (A–G) are from Figure 3. (H)

Histogram of *ire1*Δ cells expressing eroGFP, reconstituted with a 1NM-PP1-sensitized IRE1 allele, and treated with DMSO (black line), 30μM 1NM-PP1 (green line), DMSO and 1μg/ml Tm (red line), and 30μM 1NM-PP1 and 1μg/ml Tm (yellow line). Inset shows median eroGFP ratio change for each treatment. Error bars are SD of three independent experiments.

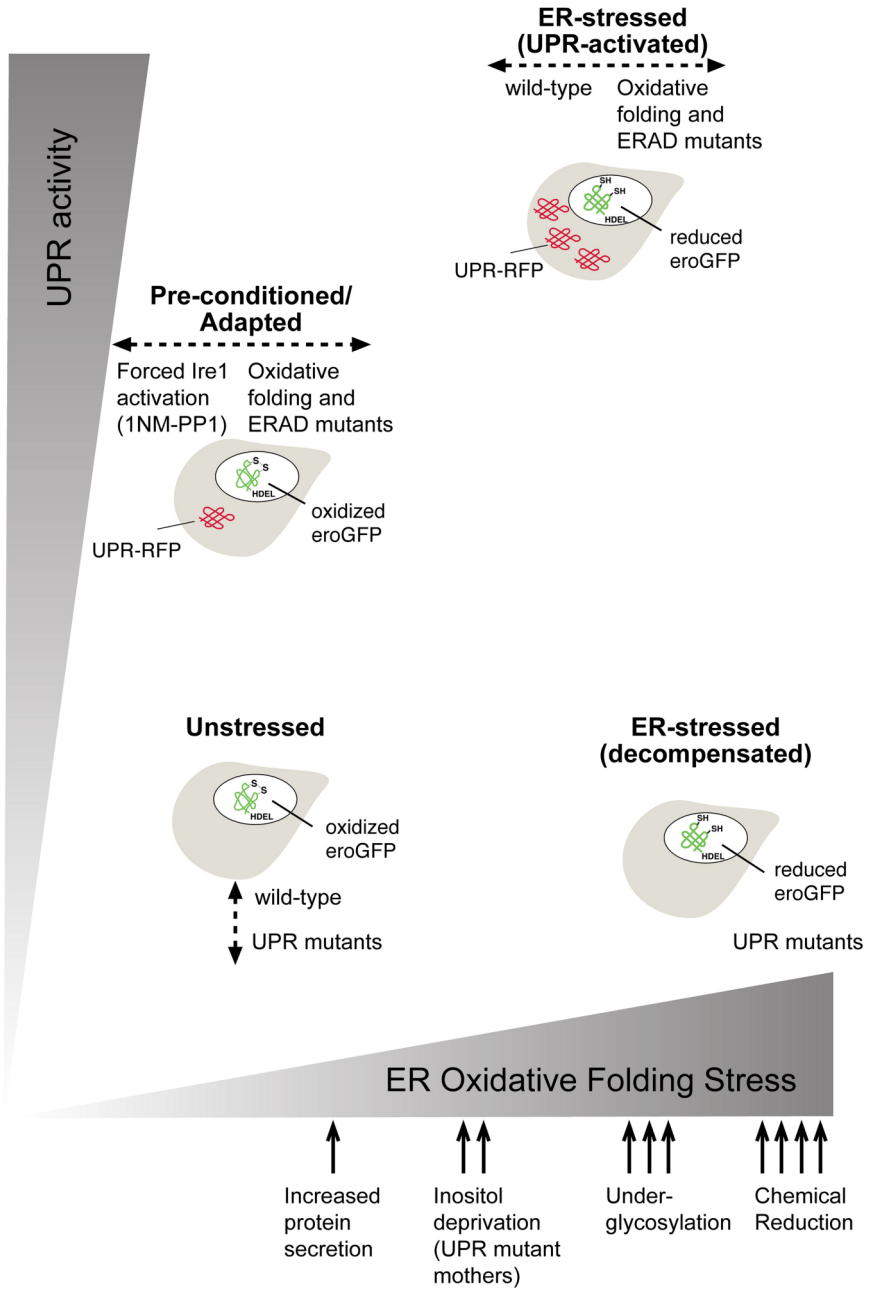

Figure 7. Conceptual model of ER stress and UPR-mediated compensation

ER oxidative folding stress, as measured by increased eroGFP ratios, can be provoked by various perturbations to ER protein folding, modification, and quality control systems. In addition, increased protein secretion and nutrient (inositol) deprivation cause ER oxidative folding stress in some cells. UPR activity, as measured by UPR-RFP, provides information on the strength of compensatory mechanisms. Triangles indicate that each variable is a continuum. Four cell states are depicted at extremes of each continuum, with positions of mutants indicated across the two variables. See text for further details.